Frequency-Dependent Polarizability of H_2 Calculated by Many-Body Theory*

Hugh P. Kelly
Department of Physics, University of Virginia, Charlottesville, Virginia 22903
(Received 10 October 1969)

Many-body perturbation theory is used to calculate the parallel and perpendicular dynamic polarizabilities of molecular hydrogen. High-order terms in the perturbation expansion are included and the poles of $\alpha(\omega)$ are calculated. Results for the dynamic dipole polarizabilities and for the molecular anisotropy are in good agreement with experiment.

I. INTRODUCTION

General discussions of time-dependent perturbations in atomic physics have been given, for example, by Karplus and Kolker[1] and by Dalgarno.[2] The use of the Brueckner-Goldstone[3,4] (BG) perturbation expansion for time-dependent perturbations has been discussed previously[5]; and applications of the BG expansion to calculate frequency-dependent atomic polarizabilities have been made for helium[6] and for atomic oxygen.[7] Both of these calculations involve the direct application of methods developed previously[8] to apply the BG expansion to atoms.

For molecules, there have been variational calculations of the dynamic dipole polarizabilities.[1,9] Recently, Dalgarno and co-workers[10-12] have used experimental data on oscillator-strength distributions, supplemented by refractive-index data and sum rules, to construct models of the dipole spectrum which reproduce dipole properties very accurately over a wide range of the spectrum.

In this paper, we use the BG many-body perturbation expansion to calculate the dipole dynamic (or frequency-dependent) polarizability of H_2. The methods used to utilize the BG expansion are those which we developed recently[13] to calculate the binding energy and static polarizabilities of H_2. These methods are essentially those developed previously for atoms.[8]

We assume a perturbing electric field $\vec{F}\cos\omega t$, so that the time-dependent perturbation is

$$V_{\rm ex}(\vec{r},t)=\cos\omega t\sum_{i=1}^{N}\vec{F}\cdot\vec{r}_i \quad , \tag{1}$$

where N is the total number of electrons. The induced electric dipole moment $\vec{p}$ is given by[5]

$$\vec{p}=\alpha(\omega)\vec{F}\cos\omega t \quad , \tag{2}$$

where $\alpha(\omega)$ is the dynamic polarizability. The full Hamiltonian is now

$$H=H_0+H_c'+V_{\rm ex} \quad , \tag{3}$$

where (in a.u.)

$$H_0=\sum_{i=1}^{N}\left[-\tfrac{1}{2}\nabla_i^2+V(r_i)\right], \tag{4}$$

and

$$H_c'=\sum_{i<j=1}^{N}r_{ij}^{-1}-\sum_{i,\alpha}Z_\alpha r_{i\alpha}^{-1}-\sum_{i=1}^{N}V(r_i) \quad . \tag{5}$$

The terms $-Z_\alpha r_{i\alpha}^{-1}$ refer to the interaction of the ith electron with the αth nucleus. The potential $V(r_i)$ refers to the single-particle potential which is introduced in order to calculate the complete set of single-particle states used in the perturbation expansion.[13] We may obtain $\alpha(\omega)$ from the relation[5]

$$\bar{E}_{\rm ex}^{(2)}=-\tfrac{1}{4}\alpha(\omega)F^2 \quad , \tag{6}$$

where $\bar{E}^{(2)}$ is the time-average energy term which has two interactions with $V_{\rm ex}$. If we write

$$V_{\rm ex}^{\pm}=\sum_{i=1}^{N}\vec{F}\cdot\vec{r}_i\tfrac{1}{2}e^{\pm i\omega t} \quad , \tag{7}$$

then $\bar{E}^{(2)}$ contains terms in which there is an interaction with $V_{\rm ex}^{\pm}$ first and then with $V_{\rm ex}^{\mp}$. If H_0 is our unperturbed Hamiltonian, then $\bar{E}^{(2)}$ is given by all terms with two interactions with $V_{\rm ex}$ and any number of interactions with H_c'. We evaluate $\bar{E}^{(2)}$ by the usual time-independent perturbation theory, except that each denominator E_0-H_0 is now $E_0-H_0-(p-q)\omega$, where p is the number of interactions with $V_{\rm ex}^{+}$ which have occurred to the right in the perturbation expression, and q is the number of interactions with $V_{\rm ex}^{-}$ which have occurred to the right of the denominator.[5]

We choose the $\hat{Z}$ axis to be along the internuclear axis of H_2. For $\vec{F}=F\hat{Z}$, $\alpha(\omega)$ is written $\alpha_{\parallel}(\omega)$, and for $\vec{F}=F\hat{X}$, $\alpha(\omega)$ is written $\alpha_{\perp}(\omega)$. From now on the symbol $\alpha(\omega)$ is used for the average dynamic dipole polarizability

$$\alpha(\omega)=\tfrac{1}{3}\alpha_{\parallel}(\omega)+\tfrac{2}{3}\alpha_{\perp}(\omega) \quad . \tag{8}$$

II. SUMS OF DIAGRAMS

In the present calculations, we use the same H_0 and therefore the same set of single-particle states used previously[13] to calculate the binding energy and static dipole polarizabilities of H_2. These states were calculated in a single-center expansion in which

$$V(r) = -\frac{2}{r_>} + \int d\vec{r}\,' \frac{|\phi'_{1s}(\vec{r}\,')|^2}{|\vec{r} - \vec{r}\,'|} , \tag{9}$$

where ϕ'_{1s} is an approximation (spherically averaged) to the lowest molecular orbital.

The lowest-order contribution to $\alpha_{\parallel}(\omega)$ is given by

$$-2\sum_k |\langle k|z|1s\rangle|^2[(\epsilon_{1s} - \epsilon_k - \omega)^{-1} + (\epsilon_{1s} - \epsilon_k + \omega)^{-1}] . \tag{10}$$

The factor 2 accounts for the two 1s electrons and the summation is over all excited single-particle states k, both bound and continuum. The lowest-order contribution to $\alpha_{\perp}(\omega)$ is obtained by replacing z by x in Eq. (10). Since we have used a single-center expansion, $\alpha_{\parallel}(\omega)$ and $\alpha_{\perp}(\omega)$ are equal in lowest order. The diagram corresponding to Eq. (10) is shown in Fig. 1(a). The heavy-dot interaction is with $V_{ex}^{\pm}$. If the bottom-dot interaction is with $V_{ex}^{\pm}$, then the denominator is $\epsilon_{1s} - \epsilon_k \mp \omega$. In the next order of perturbation theory, we include terms with one interaction with H'_C as shown in Figs. 1(b)–1(f). The crossed interaction represents $-\sum V(r_i)$. Interactions of the hole and of the particle with passive unexcited states are shown in Figs. 1(c) and 1(e), respectively. In Figs. 1(f) and 1(g) the cross enclosed by a circle symbolizes interaction with the nonspherical potential

$$V_{ns} = -\sum_{i=1}^{2} \sum_{\substack{K=2 \\ K \text{ even}}}^{\infty} \frac{2r_<^K}{K+1} P_K(\cos\theta_i) , \tag{11}$$

where $r_<(r_>)$ is the lesser (greater) of r_i and $R = 0.70$, which is one-half the nuclear separation of H_2.[14] Equation (11) comes from the second term in Eq. (5) minus the $K=0$ part, which cancels with that in $V(r)$. These interactions also occur on hole lines, but for H_2 the matrix elements $\langle 1s|r_<^K/r_>^{K+1}P_K|1s\rangle$ are zero for $K \neq 0$, since the state 1s is calculated in our single-center expansion. As discussed previously,[5,8] we may include diagonal interactions on hole lines, as in Figs. 1(b) and 1(c), and also diagrams with two or more such interactions by summing a geometrical series to give the basic diagrams of Fig. 1(a) with a denominator shifted from $\epsilon_{1s} - \epsilon_k$ to

$$\epsilon_{1s} + \langle 1s1s|v|1s1s\rangle - \langle 1s1s'|v|1s1s'\rangle - \epsilon_k . \tag{12}$$

Similarly, when we consider bound excited states, we may include diagrams 1(d)–1(f) and 1(h) for $k = k'$ (bound) and higher-order diagrams with the same diagonal interactions by summing the re-

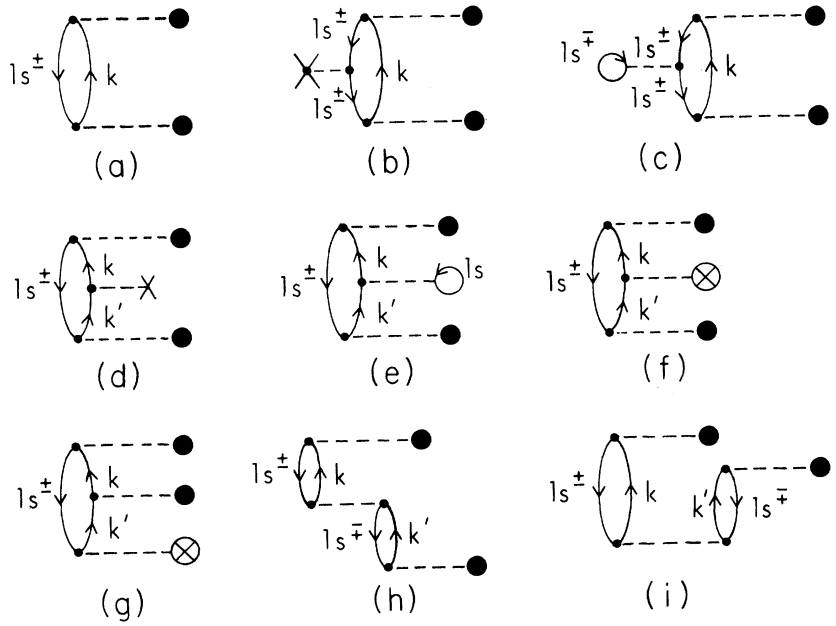

FIG. 1. Low-order diagrams contributing to $\alpha_{\parallel}(\omega)$ and $\alpha_{\perp}(\omega)$. The heavy dot represents interaction with z or x according to whether one is calculating $\alpha_{\parallel}$ or $\alpha_{\perp}$. In (f) and (g), the cross with a circle represents the interaction of Eq. (11). Diagrams (g) and (i) also occur inverted.

sulting geometric series. The result is that we obtain the basic diagram of Fig. 1(a) with the denominator $\epsilon_{1s}-\epsilon_k$ shifted to become

$$\epsilon_{1s}-[\epsilon_k+\langle k1s|v|k1s\rangle-\langle k1s'|v|k1s'\rangle + \langle k1s|v|1sk\rangle+\langle k|-(2r_<^2/r_>^3)P_2(\cos\theta)|k\rangle]. \quad (13)$$

The term $\langle 1s1s|v|k1s\rangle-\langle k1s'|v|k1s'\rangle$ accounts for the fact that the $1s$ state differs from the $1s'$ state used in V. The term $\langle k1s|v|1sk\rangle$, which is added to ϵ_k due to the diagonal interactions of Fig. 1(h), and higher-order terms due to the same interactions represents the usual positive exchange term characteristic of excited singlet states. The last term in Eq. (13) is the $K=2$ term of Eq. (11). Note that we only have the $K=2$ term in Eq. (13) since k has $l=1$, because the heavy-dot interactions in Fig. 1 are dipole interactions. The last matrix element of Eq. (13) is negative for $k(m_l=0)$ and positive for $k(m_l=\pm1)$.

This corresponds to a lowering of the energy of $1s\sigma_g np\sigma\,{}^1\Sigma_u^+$ states relative to $1s\sigma_g np\pi\,{}^1\Pi_u$. We note that our $1snp(m_l=0)$ and $1snp(m_l=\pm1)$ excited configurations correspond to $1s\sigma_g np\sigma\,{}^1\Sigma_u^+$ and $1s\sigma_g np\pi\,{}^1\Pi_u$, respectively. In Fig. 1, only diagrams 1(f) and 1(g) contribute differently to $\alpha_\parallel$ and $\alpha_\perp$. For $\alpha_\parallel$, diagrams 1(f) and 1(g) have the same sign as 1(a), and for $\alpha_\perp$, 1(f) and 1(g) are negative with respect to 1(a) when we consider that energy denominators are negative.

In the next order of perturbation theory in H_C', there are many diagrams in addition to those involving two H_C' interactions of the types shown in Figs. 1(b)–1(i). It is desirable that the poles of $\alpha_\parallel(\omega)$ and $\alpha_\perp(\omega)$ be located as accurately as possible, and in Figs. 2(a)–2(i) are shown new types of diagrams which are second order in H_C' and affect the positions of the poles. When Figs. 2(a) and 2(b) are added, the result is a product of the second-order correlation energy times the diagram of Fig. 1(a) multiplied by minus D^{-1}, where D is the denominator of Fig. 1(a).[15] This term and Fig. 1(a) are the first two terms in a geometric series which may be summed to give the diagram of Fig. 1(a) with a denominator shifted by $E_{\rm corr}(1s,1s)$, which is the correlation energy for the two ground-state electrons. Diagrams 2(c) and 2(d) add to give the product of the second-order energy (for one $1s$ electron) due to two interactions with Eq. (11) times the diagram of Fig. 1(a) multiplied by minus D^{-1}. Again we have a geometric series which may be summed to give the basic diagram of Fig. 1(a) with a denominator shifted by $\Delta E_{ns}^{(2)}$, where $\Delta E_{ns}^{(2)}$ is the total shift in energy for a single $1s$ electron due to all interactions with V_{ns}.

We can include all the shifts considered so far by replacing ϵ_{1s} and ϵ_{np} by ϵ'_{1s} and ϵ'_{np}, where

$$\epsilon'_{1s}=\epsilon_{1s}+\langle 1s1s|v|1s1s\rangle-\langle 1s1s'|v|1s1s'\rangle + E_{\rm corr}(1s,1s)+\Delta E_{ns}, \quad (14)$$

$$\epsilon'_{np}=\epsilon_{np}+\langle np1s|v|np1s\rangle-\langle np1s'|v|npl\,s'\rangle + \langle np|-\frac{2r_<^2}{r_>^3}|np\rangle+\langle np1s|v|1snp\rangle\ . \quad (15)$$

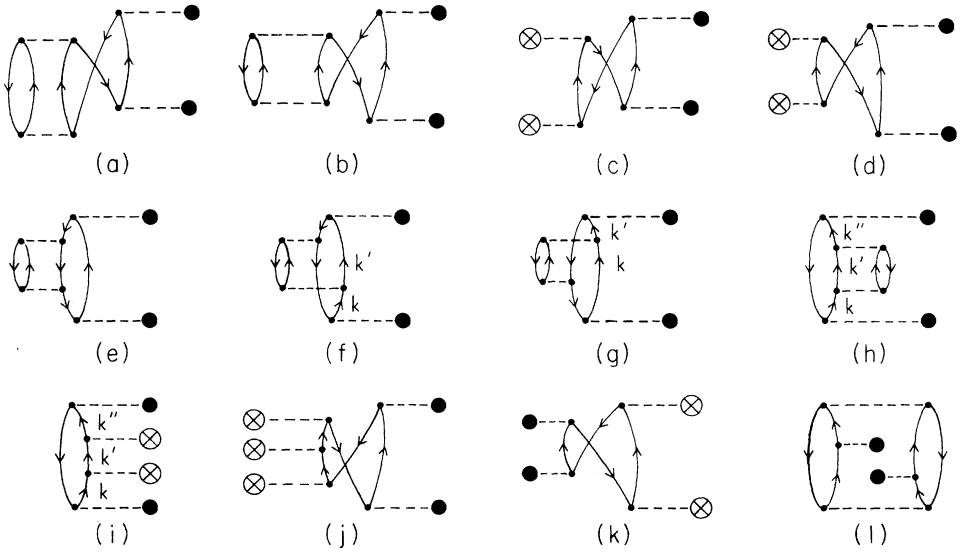

FIG. 2. Selected higher-order diagrams. The heavy dot represents interaction with the external potential given by z for $\alpha_\parallel$ and by x for $\alpha_\perp$. Diagrams (a)—(e) and (j) are included in the present calculation. Diagrams (f) and (g) are included for $k=k'=np$. Diagrams (h) and (i) are included for $k=k''=np$. Diagrams (k) and (l) are not included.

When we use ϵ'_{1s} and ϵ'_{np}, the positions of the poles of $\alpha_{\parallel}(\omega)$ and $\alpha_{\perp}(\omega)$ are given by $\epsilon'_{np} - \epsilon'_{1s}$. However, there are also contributions to the poles from the diagrams of Figs. 2(e)–2(h). In Figs. 2(f) and 2(g), these contributions occur when $k = k' = np$; and in Figs. 2(h) and 2(i), they occur when $k = k'' = np$ with $k' \neq k$. Again we have a geometric series which may be summed to give a shift $\Delta(\omega, np)$ to the denominator of Fig. 1(a). Unlike the shifts in Eqs. (14) and (15), Δ depends on ω. For example, the contribution to $\Delta(\omega, np)$ from the diagram of Fig. 2(e) is given by

$$\Delta_e^{\pm}(\omega, np) = -\sum_k \frac{|\langle k1s|v|1s1s\rangle|^2}{\epsilon_{1s} + \epsilon_{1s} - \epsilon_k - \epsilon_{np} \pm \omega}, \qquad (16)$$

where $\Delta^{\pm}$ is used according to whether $\pm\omega$ occurs in the denominator of Fig. 1(a). In higher orders of perturbation theory, shifts also occur in the denominator of Eq. (16).

When all the shifts we have discussed are included, the appropriate denominator when there is a single excitation is given by

$$D = \epsilon'_{1s} - \epsilon'_{np} + \Delta^{\pm}(\omega, np) \pm \omega. \qquad (17)$$

The poles of $\alpha_{\parallel}(\omega)$ and $\alpha_{\perp}(\omega)$ occur at the zeros of D given by Eq. (17).

TABLE I. Perpendicular dynamic dipole polarizability in a_0^3.

ω (in a.u.)	$\alpha_{\perp 2}$ [a]	$\alpha_{\perp}$ [b]	$\alpha_{\perp d}$ [c]
0.00	6.103	4.555	4.774
0.05	6.154	4.588	4.814
0.10	6.312	4.690	4.936
0.15	6.596	4.853	5.159
0.20	7.043	5.159	5.515
0.25	7.727	5.591	6.067
0.30	8.792	6.253	6.957
0.35	10.563	7.330	8.550
0.40	13.962	9.338	
0.42	16.380	10.735	
0.44	20.200	12.906	
0.46	27.219	16.826	
0.48	44.886	26.520	
0.50	198.101	109.379	
0.51	−183.507	−96.392	
0.52	−54.191	−26.525	
0.53	−26.922	−11.784	
0.54	−12.891	−4.593	

[a] Second-order except for shifted denominators.
[b] Including higher-order terms.
[c] From the model dipole spectrum of Victor and Dalgarno, Ref. 12. Values of Ref. 12 were interpolated to obtain present values.

TABLE II. Parallel dynamic dipole polarizability in a_0^3.

ω (in a.u.)	$\alpha_{\parallel 2}$ [a]	$\alpha_{\parallel}$ [b]	$\alpha_{\parallel d}$ [c]
0.00	6.390	6.502	6.803
0.05	6.450	6.562	6.872
0.10	6.638	6.749	7.092
0.15	6.978	7.088	7.492
0.20	7.527	7.633	8.146
0.25	8.392	8.489	9.201
0.30	9.812	9.887	11.017
0.35	12.412	12.428	14.672
0.40	18.538	18.351	
0.42	24.237	23.816	
0.44	37.211	36.179	
0.46	100.218	95.788	
0.48	−88.881	−84.413	
0.50	−23.307	−20.716	
0.51	−14.309	−11.975	
0.52	−7.933	−5.683	
0.53	−1.848	0.213	
0.54	7.950	−4.073	

[a] Second order except for shifted denominators.
[b] Including higher-order terms.
[c] From the model dipole spectrum of Victor and Dalgarno, Ref. 12.

III. RESULTS

The calculated perpendicular and parallel dynamic polarizabilities are listed in Tables I and II. The terms $\alpha_{\perp 2}$ and $\alpha_{\parallel 2}$ result from calculating the basic second-order diagram of Fig. 1(a) with the shifted denominator of Eq. (17), and so includes many of the higher-order terms of Figs. 1 and 2. The difference between $\alpha_{\perp 2}$ and $\alpha_{\parallel 2}$ is due to the difference between $\epsilon'_{np}(0)$ and $\epsilon'_{np}(\pm 1)$. Contributions to $\alpha_{\parallel}(\omega)$ and $\alpha_{\perp}(\omega)$ due to electron correlations come from the diagrams of Fig. 1(h) and 1(i). We have already included terms of 1(h) with $k = k' = np$ by D of Eq. (17), so these terms are now omitted. In calculating Figs. 1(h) and 1(i) we employ the shifted denominator of Eq. (17), but in the bottom denominator of Fig. 1(i) we use the shifted denominator appropriate to a double excitation.[5] It is noted that diagrams 1(h) and 1(i) are included in the coupled Hartree-Fock approximation.[5] Contributions of Figs. 1(h) and 1(i) to $\alpha_{\parallel}$ and $\alpha_{\perp}$ are identical except for differences in the shifted denominators. The interactions of Figs. 1(h) and 1(i) are repeated in higher orders, and the sum of these interactions is approximately included in this work by multiplying the basic diagram of Fig. 1(a) by the factor $(1 - R)^{-1}$, where R equals the sum of diagrams 1(h) and 1(i), all divided by diagram 1(a). By diagram 1(i), we mean the diagram actually shown plus its inverted form.

The difference between $\alpha_{\parallel}$ and $\alpha_{\perp}$ comes from interactions with V_{ns} of Eq. (11), as shown in Figs. 1(f) and 1(g), and higher-order terms. The part of Fig. 1(f) with $k=k'=np$ was already included. The remaining contributions to $\alpha_{\parallel}$ and $\alpha_{\perp}$ were explicitly evaluated. The result is an increase in $\alpha_{\parallel}$ and a decrease in $\alpha_{\perp}$. The calculations of diagrams 1(f) and 1(g) were carried out with shifted denominators. There are also higher-order terms in which Figs. 1(f) and 1(g) are modified by correlation interactions of the types shown in Figs. 1(h) and 1(i). An estimate of these effects was included by using the ratio R already determined. For Fig. 1(f), however, the correction factor is approximately $1+2R+3R^2+\cdots$. For 1(g), since k' is an excited $l=2$ state, additional calculations were carried out to obtain effects of correlations in $l=2$ states on the basic diagram 1(g). The average effect of these terms was to reduce Fig. 1(g) by approximately a factor of 0.0907. Final results for $\alpha_{\perp}$ and $\alpha_{\parallel}$ are given in the third columns of Tables I and II, respectively.

In Tables I and II, the columns labeled $\alpha_{\perp d}$ and $\alpha_{\parallel d}$ are from the model dipole spectrum of Victor and Dalgarno[12] and are expected to be accurate to 0.2%. Values given in Ref. 12 were interpolated in order to list them at our intervals. In Table III are listed the molecular anisotropy

$$\gamma(\omega)=\alpha_{\parallel}(\omega)-\alpha_{\perp}(\omega)\ , \tag{18}$$

and also $\gamma_D(\omega)$, which is the molecular anisotropy from the model dipole spectrum.[12] In all the calculations, sums over excited states were calculated by methods of Ref. 8; i.e., sums over continuum states were carried out by numerical integration, and sums over bound excited states were carried out explicitly through $n=8$ and then to ∞ by the n^{-3} rule.[8] For example, at $\omega=0$ for $\alpha_{\parallel 2}$, there is a contribution from continuum states of $1.184a_0^3$ and from bound states of $5.206\alpha_0^3$. At $\omega=0.30$, the continuum contribution is $1.420a_0^3$ and the bound contribution is $8.392a_0^3$. As ω increases, the contribution from the lowest-bound excited state becomes of increasing importance as we near the pole of $\alpha(\omega)$ caused by this excitation. In Table III, we also list $\alpha(\omega)$ defined by Eq. (8). The experimental values in the last column of Table III are interpolated from those listed by Victor and Dalgarno[12] for $\omega<0.25$. For $\omega\geq 0.25$, the model-dipole-spectrum[12] results are listed since direct experimental results are not available. In Table III, we have also listed a column α_S which is the dynamic dipole polarizability calculated with ϵ_{1S} shifted to $\epsilon_{1S}+0.0200$ a.u. We note that α_S is in better agreement with α_{expt} than is α, and this is an indication that our denominators may be in error by this amount.

In Table IV are listed the poles of $\alpha(\omega)$ which are determined by the zeros of Eq. (17). The excited states $np(0)$ and $np(\pm 1)$ correspond to the $1s\sigma_g np\sigma\,{}^1\Sigma_u^+$ and $1s\sigma_g np\pi\,{}^1\Pi_u$ molecular states, re-

TABLE III. Molecular anisotropy and dynamic dipole polarizability in a_0^3.

ω (in a.u.)	γ [a]	γ_D [b]	α_2 [c]	α [d]	α_s [e]	α_{expt} [f]
0.00	1.947	2.029	6.199	5.204	5.372	5.437
0.05	1.974	2.058	6.253	5.246	5.420	5.521
0.10	2.059	2.156	6.421	5.377	5.565	5.646
0.15	2.215	2.333	6.723	5.612	5.831	5.934
0.20	2.474	2.631	7.204	5.983	6.255	6.410
0.25	2.898	3.134	7.948	6.557	6.921	7.110
0.30	3.634	4.059	9.132	7.465	8.011	8.309
0.35	5.098	6.123	11.179	9.030	10.007	10.590
0.40	9.013		15.487	12.342	14.921	
0.42	13.081		18.999	15.096	20.161	
0.44	23.273		25.871	20.664	39.221	
0.46	78.962		51.552	43.146	−16.187	
0.48	−110.933		0.297	−10.458	50.221	
0.50	−130.095		124.298	66.014	−22.499	

[a] Molecular anisotropy given by $\alpha_{\parallel}-\alpha_{\perp}$.

[b] Molecular anisotropy as given by the model dipole spectrum of Victor and Dalgarno, Ref. 12.

[c] Dynamic dipole polarizability calculated in second order by Eq. (8) but with shifted denominators.

[d] Dynamic dipole polarizability including higher-order terms calculated by Eq. (8).

[e] Dynamic dipole polarizability calculated with ϵ_{1s} shifted by 0.020 a.u. Higher-order terms are included.

[f] Experimental values listed in Ref. 12. For $\omega\geq 0.25$, values listed are from the model dipole spectrum of Ref. 12.

TABLE IV. Positions of poles of $\alpha(\omega)$ [a].

Excited state [b]	Pole [c]
$2p$ (0)	0.4700
$3p$ (0)	0.5508
$4p$ (0)	0.5782
$5p$ (0)	0.5894
$6p$ (0)	0.5954
$7p$ (0)	0.5990
$8p$ (0)	0.6013
$2p$ (± 1)	0.5050
$3p$ (± 1)	0.5608
$4p$ (± 1)	0.5816
$5p$ (± 1)	0.5911
$6p$ (± 1)	0.5963
$7p$ (± 1)	0.5996
$8p$ (± 1)	0.6018

[a]Excitation energy from ground state in a.u. due to $1s \rightarrow np$ excitations.

[b]States $np(0)$ correspond to molecular excited states $1s\sigma_g np\sigma_u\, {}^1\Sigma_u^+$, and states $np(\pm 1)$ correspond to molecular states $1s\sigma_g np\pi_u\, {}^1\Pi_u$.

[c]Values of ω for which Eq. (17) equals zero.

spectively. The $1s \rightarrow np(0)$ excitations are associated with the poles of $\alpha_{\parallel}(\omega)$ and $1s \rightarrow np(\pm 1)$ excitations are associated with poles of $\alpha_{\perp}(\omega)$. Considering the improvement in α_S over α, we suspect that our values for the poles of $\alpha(\omega)$ generally may be too high by 0.020 to 0.025 a.u.

In carrying out these calculations we have used the Born-Oppenheimer approximation[16] and neglected the nuclear motion. Our excited states were also calculated at the fixed nuclear equilibrium separation of the ground state which is consistent with the Franck-Condon principle.[17] We note [18] that the potential curve for the ground state of H_2 is deep compared to those for the ${}^1\Sigma_u^+$ and ${}^1\Pi_u$ excited states of this calculation. The nuclear vibration frequency of the ground state is 4395 cm^{-1} or 0.020025 a.u.,[18] and so the vibrational energy of the ground state is 0.01001 a.u. Our neglect of vibrational effects may then account for some of the error in our value for $\alpha(\omega)$ as compared with the experimental value in Table III. Other errors may come from neglect of higher-order diagrams and from the approximations we have used to include those higher-order diagrams which were considered. Examples of fourth-order diagrams which were not included are shown in Figs. 2(k) and 2(l). Future calculations will include additional diagrams and vibrational effects.

ACKNOWLEDGMENTS

I wish to acknowledge helpful discussion with Professor V. Celli, Professor G. Hess, Professor H. Jehle, and Professor P. Schatz. I am also grateful for the assistance of Professor Alan Batson and his staff at the Computer Science Center of the University of Virginia.

*Work supported in part by the Aerospace Research Laboratories, Office of Aerospace Research, U.S. Air Force Contract No. F33615-69-C-1048.

[1]M. Karplus and H. J. Kolker, J. Chem. Phys. 39, 1493 (1963); 41, 880 (1964); 41, 3955 (1964).

[2]A. Dalgarno, in Perturbation Theory and Its Applications in Quantum Mechanics, edited by C. H. Wilcox (J. Wiley & Sons, Inc., New York, 1966), p. 145.

[3]K. A. Brueckner, Phys. Rev. 97, 1353 (1955); 100, 36 (1955); and The Many-Body Problem (John Wiley & Sons, Inc., New York, 1959).

[4]J. Goldstone, Proc. Roy. Soc. (London) A239, 267 (1957).

[5]H. P. Kelly, University of Virginia Report, 1966 (unpublished); Correlation Structure in Atoms, Advances in Theoretical Physics (Academic Press Inc., New York, 1968) Vol. 2, p. 75.

[6]N. C. Dutta, T. Ishihara, C. Matsubara, T. P. Das, and R. T. Pu, Phys. Rev. Letters 22, 8 (1969).

[7]H. P. Kelly, Phys. Rev. 182, 84 (1969).

[8]H. P. Kelly, Phys. Rev. 131, 684 (1963); 136, B896 (1964); 144, 39 (1966).

[9]G. A. Victor, J. C. Browne, and A. Dalgarno, Proc. Phys. Soc. (London) 92, 42 (1967).

[10]A. Dalgarno and W. D. Davison, Adv. At. Mol. Phys. 2, 1 (1966).

[11]A. Dalgarno, T. Degges, and D. A. Williams, Proc. Phys. Soc. (London) 92, 291 (1967).

[12]G. A. Victor and A. Dalgarno, J. Chem. Phys. 50, 2535 (1969).

[13]H. P. Kelly, Phys. Rev. Letters 23, 455 (1969).

[14]W. Kolos and L. Wolniewicz, J. Chem. Phys. 41, 3663 (1964).

[15]H. P. Kelly, Phys. Rev. 134, A1450 (1964).

[16]M. Born and J. R. Oppenheimer, Ann. Physik (Leipzig) 84, 457 (1927).

[17]E. U. Condon, Phys. Rev. 28, 1182 (1926).

[18]W. Kauzmann, Quantum Chemistry (Academic Press Inc., New York, 1957), p. 397.